Earth and Planetary Science Letters xxx (2010) xxx–xxx

Contents lists available at ScienceDirect

Earth and Planetary Science Letters

journal homepage: www.elsevier.com/locate/epsl

Testing the accuracy of absolute intensity estimates of the ancient geomagnetic field using copper slag material

Ron Shaar [a,*], Hagai Ron [a], Lisa Tauxe [b], Ronit Kessel [a], Amotz Agnon [a], Erez Ben-Yosef [c], Joshua M. Feinberg [d]

[a] The Institute of Earth Sciences, The Hebrew University of Jerusalem, Givat Ram, Jerusalem, 91904, Israel
[b] Scripps Institution of Oceanography, University of California, San Diego, La Jolla, CA, 92093-0220, USA
[c] Department of Anthropology, University of California, San Diego, La Jolla, CA, 92093-0532, USA
[d] Institute for Rock Magnetism, Department of Geology and Geophysics, University of Minnesota, Minneapolis, MN 55455-0231, USA

ARTICLE INFO

Article history:
Received 13 August 2009
Received in revised form 4 December 2009
Accepted 8 December 2009
Available online xxxx

Editor: P. DeMenocal

Keywords:
paleointensity
archeomagnetism
slag
rock magnetism
Thellier method
jacobsite

ABSTRACT

The Middle-Eastern copper slag is a promising new material for studying intensity variations in the geomagnetic field with high resolution and precision. The purpose of this study is to test the accuracy of archaeointensity estimates determined using copper slag by addressing two questions: 1) "Does slag material display the magnetic properties required for valid Thellier experiments?" and 2) "What is the accuracy of the archaeointensity estimates derived from Thellier-style experiments on optimal samples?" We address the first question through a comprehensive microscopic and magnetic study of representative archaeological slag samples in order to identify the properties responsible for optimal behavior in Thellier experiments. To address the second question, we reproduced slag samples in the laboratory under controlled magnetic fields and analyzed them using the same IZZI paleointensity technique used for the ancient slag. Microscopic analyses of the archaeological slag show that ferromagnetic phases occur as three-dimensional dendritic structures whose branches consist of submicron-elongated particles. Magnetic analyses show that these dendrites behave as an assemblage of shape-controlled, single-domain-like particles and that their magnetization is thermoremanent. We conclude that slag material can be magnetically suitable for valid Thellier experiments. The laboratory-produced slag material demonstrated similar magnetic and mineralogical properties as the archaeological slag. IZZI experiments showed that non-linear TRM acquisition, even at field strengths similar to Earth's, and TRM anisotropy are important factors to monitor during paleointensity studies of slag material. Anisotropy and non-linearity are probably related to the dendritic shape of the oxide grains. Intensity estimates derived from three laboratory-produced slag samples demonstrated accuracy to within ~5% after applying the required corrections.

1. Introduction

The behavior of the ancient geomagnetic field is one of the few available probes for investigating Earth's deep interior through time. By studying the past strength of the geomagnetic field, or paleointensity, we gain information useful for constraining possible modes of fluid motion in the outer core (Glatzmaier et al., 1999; Selkin and Tauxe, 2000; Johnson et al., 2003; Gubbins et al., 2006; Tarduno et al., 2006). The ultimate aim of paleointensity studies is to establish a well-documented history of geomagnetic intensity changes. Yet, some of the most basic questions remain elusive, such as "How fast can the field change?", and "How strong or weak can the field get?" (Tauxe, 2006; Tauxe and Yamazaki, 2007; Ben-Yosef et al., submitted for publication). Archaeointensity data, covering the past few thousand years, can help answer these fundamental questions by documenting the high-frequency features of the field as recorded by archaeological artifacts. High-resolution archaeointensity investigations are key to documenting short-term events (Gallet et al., 2003; Ben-Yosef et al., 2008a,b; Ben-Yosef et al., submitted for publication; Genevey et al., 2009) and require accurate data that are linked to precise age determinations.

Paleointensity studies frequently rely on the Thellier method (Thellier and Thellier, 1959), which is the most accepted and widely used absolute paleointensity technique (Valet, 2003; Tauxe, 2009). The Thellier method includes a gradual replacement of the sample's original remanent magnetization (NRM) with a laboratory thermoremanent magnetization (TRM) acquired in a known field. This procedure should provide an accurate estimate of the ancient field in which the NRM was acquired, presuming a very strict condition: the sample must retain a TRM carried exclusively by non-interacting single-domain (or quasi-single domain) particles (Tauxe, 2009; Dunlop and Özdemir, 1997).

Accurate paleointensity estimates are very difficult to obtain, mainly because suitable materials for valid Thellier experiments are rare. Most materials contain a dominant non-single domain phase, or carry a significant portion of a remanence of non-thermal origin, such as viscous (VRM) or chemical (CRM) magnetization. In addition, the magnetic properties of the primary remanence carriers may later be chemically or

* Corresponding author. Tel.: +972 2 6586856; fax: +972 2 5662581.
E-mail address: ron.shaar@mail.huji.ac.il (R. Shaar).

0012-821X/$ – see front matter © 2009 Elsevier B.V. All rights reserved.
doi:10.1016/j.epsl.2009.12.022

physically altered by natural processes or by the multiple heating steps inherent in a Thellier-style experiment. As a result, much effort has been focused on finding suitable materials and demonstrating the validity of the intensity estimates obtained from them.

Ben-Yosef et al. (2008a,b) and Ben-Yosef et al. (submitted for publication) recently introduced Middle-Eastern copper slag as a promising new material for archaeointensity studies. Copper slag material is a remnant of the ancient copper industry that flourished in the Middle East for thousands of years starting in the Chalcolithic period (4500 BCE) and extending through the Islamic period (1516 CE). Slag is a waste material from the smelting process, by which copper ores (and fluxes) were heated in a furnace to temperatures of 1200 °C, until a separation between metallic copper and the rest of the melt was achieved. During this process the residual melt lying on top of the copper was removed by letting it solidify in the furnace or by breaking the furnace's walls and letting it pour out. Occasionally, this melt trapped charcoal fragments before solidifying as a slag. In some sites large quantities of slag accumulated in waste-piles. Some of these piles were deposited at a relatively fast rate reaching up to 2 m per century (Levy et al., 2008; Ben-Yosef et al., submitted for publication).

Copper slag has a number of magnetic properties that make it a promising material for archaeointensity studies: 1) The magnetization is thermoremanent with a strong intensity typically on the order of a few A m^2/kg. 2) Rapid cooling in air produces glassy textures with sub-micrometer grains at the outer margin of the slag, often in the size range of single-domain particles. 3) The cooling rate experienced by the slag after smelting is of the same order of magnitude as the cooling rate applied during Thellier experiments. Therefore, "cooling rate corrections" (Fox and Aitken, 1980; Halgedahl et al., 1980) that compensate for differences in cooling rates are insignificant. 4) Embedded charcoal fragments in the slag enable direct and independent radiocarbon dating of magnetic remanence acquisition. 5) Stratified archaeological cross-sections of slag and charcoals (e.g. Levy et al., 2008; Ben-Yosef et al., submitted for publication) allow for a unique continuous high-resolution intensity record with a potential time resolution of tens of years.

The objective of this work is to thoroughly test the accuracy of archaeointensity estimates determined using copper slag. This study aims to answer two fundamental questions: 1) "Does slag material display the magnetic properties required for valid Thellier experiments?" And 2) "What is the accuracy of the archaeointensity estimates derived from Thellier-style experiments on optimal samples?". The first question is addressed by a comprehensive magnetic and electron microscopy study of archaeological slag samples that display excellent behavior in Thellier-style experiments. This portion of the study identifies the mineralogy of the ferromagnetic phases, characterizes their magnetic domain state, and finds the magneto-mineralogical qualities of the most successful samples. To test the accuracy of archaeointensity estimates from copper slag we conducted an empirical test using the IZZI protocol on synthetic copper slag samples produced under laboratory controlled sets of magnetic field. The experimental set up allowed us to create samples with similar magnetic properties as in archaeological slag. We analyzed these samples using the very same paleointensity procedures used for the ancient slag in order to quantify the accuracy of the paleointensity procedure in general.

2. Methods

2.1. Archaeological sample set collection

The archaeological sample set for the present study was collected from an exposed section in a 2 m pile of slag, at the excavated site of Timna-30, the Arava valley, southern Israel (see supplementary material, Fig. S1 and Ben-Yosef et al., 2008b for location map). According to excavators, the ages of the exposed sequence span from early 14th century BCE at the bottom, to the 10th century BCE at the top (Rothenberg, 1980). Following Ben-Yosef et al. (2008b, submitted for publication), we classified the slag material in the exposed profile into two groups according to stratigraphic level. The upper part of the pile, labeled in this paper group A, contains massive flat shaped slag, 10 to 40 cm in diameter, and 5 to 10 cm in thickness. Colors in fresh cross-sections are black or dark gray with yellowish and whitish areas. Glassy textures are visible in the rim, and flow textures on the upper side of the slag give it an appearance resembling a small-scaled Pahoehoe lava-flow (see Fig. 7a–f in Ben-Yosef et al., 2008b). The slag fragments in the lower part of the pile, labeled in this paper group B, are irregularly shaped with sizes between 5 and 15 cm. Textures are variable, ranging from glass-droplets to vesicular glass to aphanitic textures (see Fig. 4 in Ben-Yosef et al., 2008b). In some instances, needle-shaped phenocrysts ~1 mm long are visible. Slag from both groups show no visible signs of alteration and charcoal fragments are frequently embedded in them.

For a preliminary study, nine samples from the two groups were collected from different relative heights (Fig. S1 in supplementary material) and were analyzed using an absolute paleointensity IZZI (Tauxe and Staudigel, 2004) protocol. The five samples showing the best behavior in the IZZI experiments were selected for further analyses and are reported in this study. The sample set consists of one sample from group A (IS26C) and four samples from group B (IS26E-G, I). A further paleointensity study of site Timna-30 including an archaeological excavation designed especially for high-resolution sampling of slag is currently in progress.

2.2. Re-melting experiments

The purpose of the re-melting experiments was to empirically quantify the accuracy of paleointensity estimates derived from the slag material using the IZZI protocol. The experiments were carried out in the experimental petrology laboratory at the Institute of Earth Sciences, Hebrew University of Jerusalem. The experimental setup built for this study is shown in Fig. S2 in the supplementary material. Starting material was a crushed slag from site Timna-28, located a few kilometers south of site Timna-30. The crushed slag was put in laboratory-built crucibles made from a fire-resistant brick material machined into cylindrical shapes with an inner diameter of 1.5 cm and a height of 2.5 cm. A thermocouple was assembled on the bottom of the crucible so that sample temperatures could be digitally recorded throughout the experiments. The crucible was fixed on an alumina rod and inserted into a Carbolite 1-atm tube furnace. The rod allowed us to lower the crucible from the furnace's hot spot to a cooling chamber located below the furnace. The cooling chamber was built as an extension of the furnace's tube. A system of three-axis Helmholtz coils, connected to three DC current sources, was used to control the magnetic field inside the cooling chamber. The field in the cooling chamber was measured in four positions using an Applied Physics APS-520 three-axis fluxgate magnetometer, thereby allowing estimation of uncertainty in the field.

Preliminary experiments showed that the crushed slag melts completely after 1 h at 1300 °C. Quenching the melt by rapid cooling outside the furnace yielded a glassy material with very weak and unstable magnetic signal. Scanned Electron Microscopy (SEM) analysis of the glass showed no visible crystals. Additional experiments showed that different types of crystals form when slower cooling rates are applied between 1300 °C and 1000 °C. The final and most suitable experimental procedure found in this preliminary work included three stages (supplementary material, Fig. S2): First, a crushed archaeological slag was heated to 1300 °C for 1 h in order to guarantee complete melting. Then, the melt was cooled to 1000 °C using a controlled, constant cooling rate. Finally, when the temperature reached 1000 °C, the sample was lowered to a cooling chamber below the furnace, into a predetermined stable magnetic field.

Please cite this article as: Shaar, R., et al., Testing the accuracy of absolute intensity estimates of the ancient geomagnetic field using copper slag material, Earth Planet. Sci. Lett. (2010), doi:10.1016/j.epsl.2009.12.022

Our re-melting experiments were run under a wide range of cooling rates and magnetic field intensities. Since the ancient cooling rate is unknown, we compared the microscopic properties of the re-melted material and those of the archaeological material, in order to find the most suitable cooling rate. Samples produced under a cooling rate of 130 °C/min showed the most similarity to the archaeological samples in terms of magneto-mineralogy, magnetic domain state, and grain size. Therefore, the sample set for this study consisted of three samples produced under a cooling rate of 130 °C/min and a laboratory field of 30, 60 and 90 μT (samples RS25, RS26, and RS27, respectively).

2.3. Electron microscopic analysis

Polished sections of archaeological and laboratory-produced slag were prepared from fresh samples and from specimens that had undergone full Thellier experiments. The samples were analyzed for grain size, texture, and composition of the magnetic particles at the Unit for Nanoscopic Characterization, the Hebrew University of Jerusalem. Chemical compositions were measured in backscatter mode using a FEI Quanta 200 environmental SEM equipped with EDS detector, and a FEI Sirion high-resolution SEM. Crystallographic information on the silicate and oxide mineralogy within the slag samples was obtained from polished sections using a JEOL 6500 field emission gun (FEG-SEM) outfitted with an HKL electron backscatter diffraction (EBSD) detector at the University of Minnesota. EBSD measurements were conducted using an operating voltage of 20 keV and a working distance of 25 mm. Minerals were identified by indexing diffraction patterns using Channel 5 software. Crystallographic solutions were accepted only if the mean angular deviation (MAD) value was less than 1.4°.

2.4. Magnetic characterization

A pair of specimens from each archaeological sample and from one re-melted sample was analyzed for rock magnetic characterization at the Institute for Rock Magnetism (IRM), University of Minnesota. Each pair included one specimen that had undergone a successful paleointensity experiment and one fresh specimen that had never been heated. The rock magnetic analyses were designed to characterize the remanence carriers in terms of magnetic mineralogy, domain state and type of magnetization (i.e. test the assumption of TRM as the exclusive source of magnetization).

Curie temperatures were determined using two approaches: Strong-field thermomagnetic curves (*M–T* curves), measured in a helium atmosphere on a Princeton Measurements Vibrating Sample Magnetometer (μVSM) equipped with a furnace, and low-field susceptibility curves (*K–T* curves), measured on a Geofyzika KLY-2 KappaBridge AC Susceptibility Bridge in an argon atmosphere. Additional information about the magnetic mineralogy and domain state was collected from observations of low-temperature transitions measured using a Quantum Designs Magnetic Properties Measurements System (MPMS). SIRM remanence acquired by specimens at low temperature was measured twice: once after cooling from 300 to 10 K in zero field ("zero field-cooled", ZFC), and a second time after cooling from 300 to 10 K in a 2T field ("field-cooled", FC). The stability of TRM in low temperatures ("low-temperature memory") was measured during a cooling–heating cycle from 300 K to 10 K back to 300 K, on the MPMS, in order to help characterize the particles involved in TRM acquisition. Temperature dependence of low-field susceptibility was measured on the MPMS at three frequencies: 1, 10, and 100 Hz, in order to help characterize any superparamagnetic phases. Room-temperature hysteresis loops and backfield curves were collected for the specimens that passed the Thellier experiments on the μVSM. The hysteresis parameters of saturation magnetization (M_s), saturation remanence (M_{rs}), coercivity (B_c) and coercivity of remanence (B_{cr}) were estimated from the hysteresis loops and the backfield curves using the techniques described in Tauxe (2009).

2.5. Absolute paleointensity experiments

Six small chips, 1 to 5 mm in size, were isolated from the glassy outer margin of each archaeological sample, five for the paleointensity experiments and one for a preliminary AF demagnetization experiment. AF demagnetization served as a selection test for the samples, and only those samples with orthogonal projection plots converging towards the origin were chosen for further study. In addition, all specimens used in this study had NRMs $>10^{-7}$ A m^2. Specimens for the paleointensity procedure were prepared by wrapping chips with glass microfiber filters, and gluing them inside 12-mm diameter glass vials using potassium-silicate glue (KASIL).

Absolute paleointensity experiments were performed at the palaeomagnetic laboratory at the Institute of Earth Sciences, the Hebrew University of Jerusalem, using a 2G cryogenic magnetometer and an upgraded version of an ASC-TD48 thermal demagnetizer oven. The commercial ASC oven was modified for paleointensity experiments by wrapping an additional coil around the oven for inducing a DC magnetic field. In addition, temperature controllers were upgraded to Watlow-Series-96 controllers for digital communication. A laboratory-built LabView software package was used to control the heating parameters and monitor the temperature throughout the experiments. We calibrated the system by placing additional five thermocouples at different locations in the sample boat region of the oven. Calibration procedures were repeated until we achieved an accuracy of better than ±2 °C, a heating overshoot of less than 1 °C, and excellent reproducibility of the heating process.

The absolute paleointensity experiments followed the IZZI protocol of Tauxe and Staudigel (2004 and Tauxe, 2009). Routine checks of the reproducibility of partial thermal remanence acquisition (pTRM checks) were applied every second temperature step. Paleointensity estimates were corrected for anisotropy using TRM anisotropy tensor (ATRM), which was calculated through the acquisition of TRM in six positions ($x,-x,y,-y,z,-z$) in the specimen's coordinate system using an oven field of 40 μT or 90 μT. ATRM procedure was monitored by comparing intensities acquired at opposite positions, while specimens with a difference larger than 6% were rejected. In addition, non-linear TRM (NLT) behavior (Selkin et al., 2007) was checked through acquisition of TRM at different field intensities, ranging from 20 to 100 μT. Alterations of the magnetic properties during the ATRM and NLT procedures were monitored by additional TRM acquisition tests at the end of each procedure, performed using similar conditions as the first TRM acquisition (i.e. temperature, field intensity and position), while specimens with a difference larger than 6% were rejected.

3. Results

3.1. Electron microscope analysis

Representative SEM images of group A slag are shown in Fig. 1a–b. These show three phases: Mn–Fe oxides arranged in a dendritic texture (light gray), pure copper droplets (bright white), and a silicate matrix (dark gray). The dendrites feature parallel rod-shaped sections a few microns in length and submicrons in widths. EBSD patterns collected from the dendrites could be successfully indexed as magnetite, indicating an isometric crystalline structure. EBSD patterns collected from different branches of the same dendrite displayed identical orientations, indicating that the dendrite is essentially an ornately shaped single crystal. The dimensions of the dendrite branches were smaller than the EDS sampling volume, and thus hindered direct compositional analysis. A sample EDS spectrum is shown in Fig. 2 and consists most notably of Al, Fe, Mg, and Mn. We assume that the Si and Ca in the EDS spectra are associated with the surrounding silicate matrix. In an effort to estimate the composition of the dendritic material we subtract the composition of the background silicate matrix from the composition of the dendritic areas. This rough approximation suggests a

Please cite this article as: Shaar, R., et al., Testing the accuracy of absolute intensity estimates of the ancient geomagnetic field using copper slag material, Earth Planet. Sci. Lett. (2010), doi:10.1016/j.epsl.2009.12.022

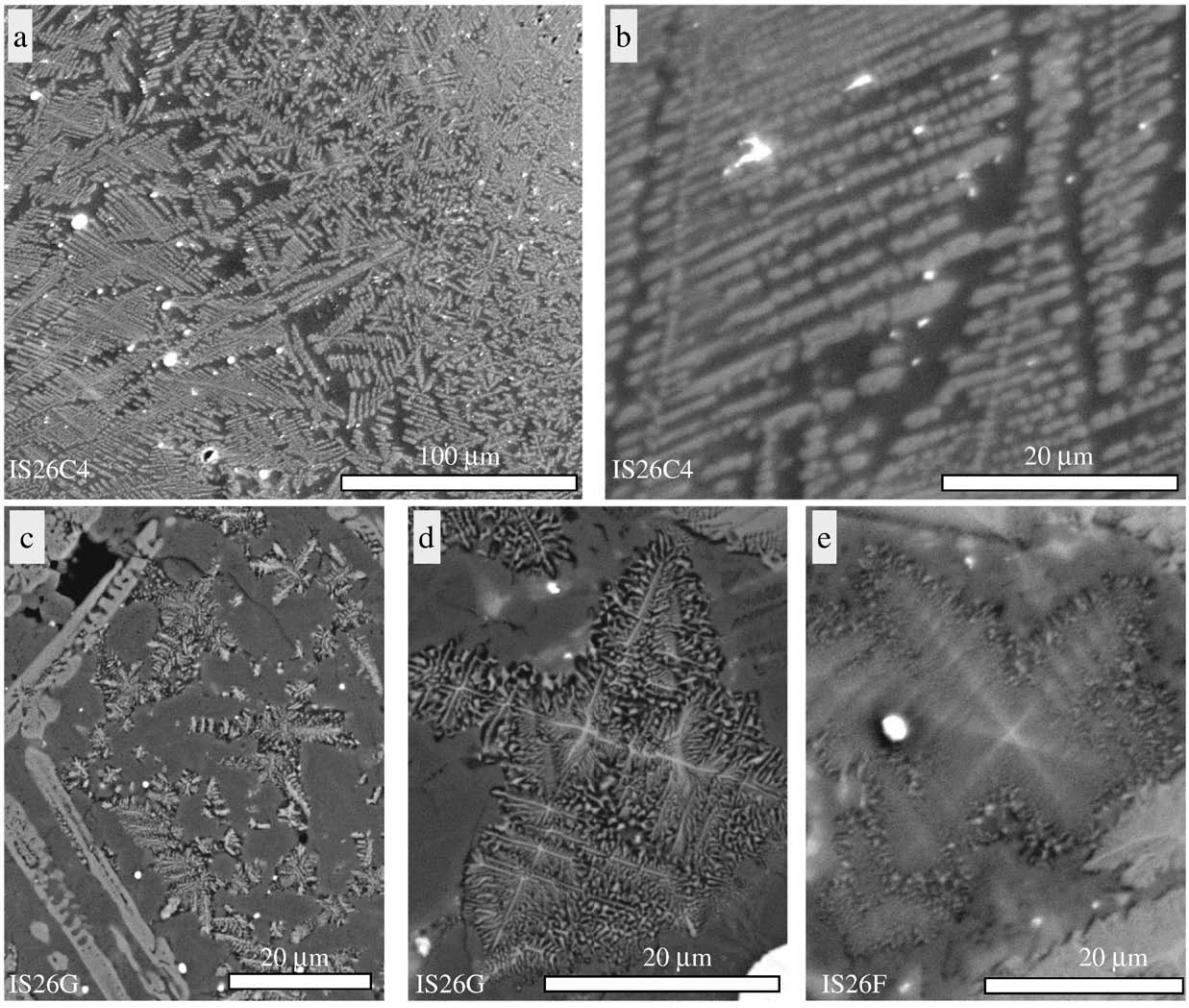

Fig. 1. Representative backscattered electron images of archaeological slag. (a)–(b) Textures of group A slag. The slag contains three phases: Mn–Fe oxides arranged in a dendritic texture (light gray), pure copper droplets (bright white), and a silicate matrix (dark gray). (c)–(e) Textures of group B slag. Slag contains large needle-shaped silicate phenocrysts, copper droplets (bright white), Fe oxides arranged in a dendritic texture (light gray), and a silicate matrix (dark gray).

chemical composition of $Fe_{3-x}(Al,Mn,Mg)_xO_4$, where $0.6<x<1.4$ (see Section 3.2 for mineralogical identification). EBSD patterns collected from the silicate matrix indicate the presence of enstatite and wollastonite. The close association of these two minerals has been observed before (Ohashi, 1984) and a similar assemblage of silicate and Mn–Fe oxide minerals was reported in an X-ray diffraction study of industrial "silicomanganese" slag castings (Min'ko et al., 1988).

Figs. 1c–e and 3a–b show representative SEM images of group B slag. The slag from group B contains four phases: large needle-shaped silicate phenocrysts, copper droplets (bright white), Fe oxides arranged in a dendrite texture (light gray), and a silicate matrix (dark gray or black areas). EBSD patterns from the large needle-shaped silicates were successfully indexed as forsteritic olivine, while the dark gray silicate matrix located immediately around the dendrites was indexed as diopside. The dendrites, which were indexed as magnetite, appear in symmetrical arrays of rods, with 2-fold or 3-fold symmetry. As in the case of the group A slag samples, EBSD patterns collected from different branches of the oxide dendrites displayed identical crystallographic orientations, indicating the single-crystal nature of the dendrites. The dendrites grow to dimensions of a few microns to tens of microns, and are bound by the diopside matrix or by the forsterite phenocrysts. The chemical composition is estimated as $Fe_{3-x}(Al,Mg)_xO_4$, where $x \ll 1$.

Fig. 3 shows that the re-melted slag reproduces the textures seen in group B samples. EBSD patterns collected from the light-gray silicate dendrites visible behind the oxide dendrite in Fig. 3c were indexed as diopside and enstatite. Chemical composition of the dendrites is estimated as $Fe_{3-x}(Al,Mn,Mg)_xO_4$, where $x \ll 1$.

3.2. Magneto-mineralogical characterization

Curie temperatures (T_c) were calculated using three styles of differential methods described by Tauxe (1998): 1) maximum in the second derivative of *M–T* curve, 2) maximum in the first derivative of *K–T* curve, and 3) maximum in the second derivative of *K–T* curve. The results are given in Table 1. Representative results showing reversible heating and cooling curves are presented in Fig. 4. Curie temperatures calculated using the *M–T* curves are inconsistent with the unblocking temperatures obtained from the Thellier experiments (Table 1), and apparently underestimate T_c. This underestimation may result from the presence of a dominant paramagnetic phase which masks the sharp drop at T_c. T_c determinations, calculated using the *K–T* curves, are therefore 376–386 °C, 551–564 °C and 528 °C for group A, group B, and re-melted slag respectively.

Fig. 5a,b shows low-temperature remanence measurements for representative samples. None of the measurements show the Verwey transition at 120°K or the isotropic point at 130°K. Therefore, the presence of stoichiometric magnetite can be excluded. Instead, we observe an abrupt change in remanence at lower temperatures in both the field-cooled (FC) and zero-field cooled (ZFC) warming curves. This temperature is designated as T_R and is in the range of 50 to 70°K for

Please cite this article as: Shaar, R., et al., Testing the accuracy of absolute intensity estimates of the ancient geomagnetic field using copper slag material, Earth Planet. Sci. Lett. (2010), doi:10.1016/j.epsl.2009.12.022

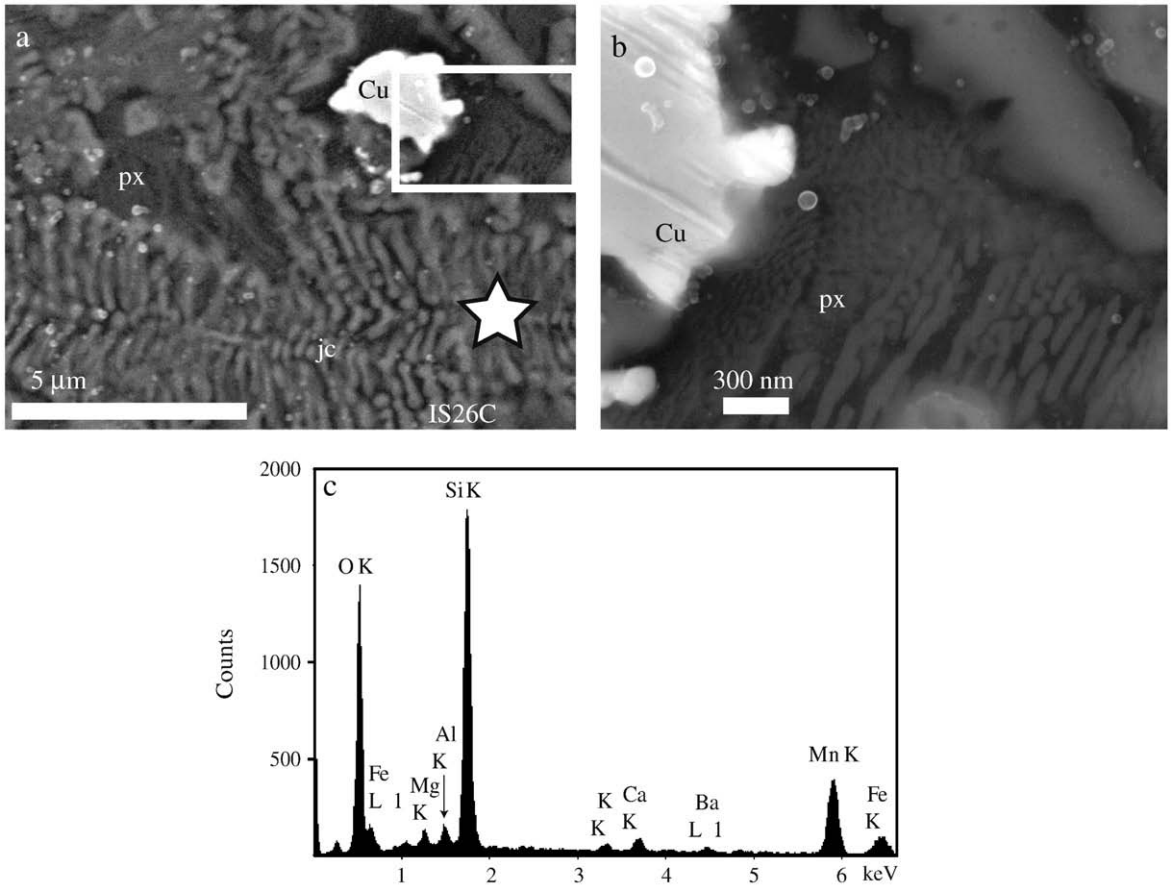

Fig. 2. Electron microscope analysis of group A slag. (a) Backscattered electron image of Group A slag showing copper droplets (Cu), dendrites of strongly magnetic, isometric, Mn-rich oxide (jc), and intergrowths of enstatite and wollastonite (px). (b) A magnified view of the intergrowths of enstatite and wollastonite adjacent to the copper droplet. c) EDS compositional measurement of the Mn-rich oxide. The star in (a) indicates the location of the measurement.

group B, and in the range of 50° to 100°K for the re-melted slag (Fig. 5a, b). Fig. 5c,d shows in-phase and out-of-phase low-temperature susceptibility. The in-phase susceptibility at T_R is at a local maximum and drops sharply below it. This behavior was previously reported for non-stoichiometric titanomagnetites (Özdemir et al., 1993; Moskowitz et al., 1998; Brachfeld and Hammer, 2006) and is interpreted here as a result of a low substitution of Al, Mn or Mg in magnetite.

Combining the magnetic and chemical analyses, we can identify the magnetic mineralogy of the slag (Table 1). The microscopic characterization of group A suggests an isometric oxide with a chemical composition of $Fe_{3-x}(Al,Mn,Mg)_xO_4$. The value of x estimated from the chemical analysis is $0.6<x<1.4$, whereas the observed Curie temperatures suggest a more tightly constrained value of $0.7<x<0.8$ (Vautier and Paulus, 1970). We consider the magnetic analysis to be more reliable than the chemical composition estimate because of the small dimensions of the grains and therefore argue for values of x in the range of $0.7<x<0.8$. The composition of the ferromagnetic phase in group A is a solid solution of magnetite (Fe_3O_4), jacobsite ($MnFe_2O_4$), and galaxite [$(Mn,Mg)(Al,Fe)_2O_4$], with a composition closest to that of jacobsite. Such solid-solutions are common in natural metamorphic rocks (Essene and Peacor, 1983; Beard and Tracy, 2002) and no miscibility gaps are thought to exist along the join between these minerals at low temperatures. The ferromagnetic phase in group B slag is magnetite with low substitution of Al or Mg. The ferromagnetic phase of the re-melted slag is magnetite with a low substitution of Al, Mn or Mg. Both the chemical analyses and Curie temperatures indicate a higher degree of substitution for the re-melted slag, and we explain this difference by an increased concentration of Fe in group B due to the crystallization of needle-shaped olivine phenocrysts.

3.3. Magnetic domain state

Representative hysteresis loops, and hysteresis parameters displayed on a Day plot (Day et al., 1977) are shown in Fig. 6. Hysteresis parameters of group A and group B fall within the pseudo-single domain (PSD) range, while group A falls higher in the PSD field, and above it. Hysteresis parameters of the re-melted samples are scattered along a straight line through the multi-domain (MD) and the PSD fields, towards the single-domain (SD) field. This behavior is a characteristic of bi-modal mixture of SD and superparamagnetic (SP) grains (Dunlop, 2002; Dunlop and Carter-Stiglitz, 2006).

Additional observations about the samples' domain states were obtained from low-temperature FC and ZFC remanence curves (Fig. 5b), and from measurements of frequency and temperature dependence of low-field susceptibility (Fig. 5c,d). Carter-Stiglitz et al. (2006) showed that for MD magnetite the ZFC curve is elevated over the FC curve. This behavior is not observed in any of the samples, thereby eliminating the possibility of a dominant MD phase. Worm and Jackson (1999) demonstrated that samples displaying frequency-dependence of in-phase susceptibility accompanied by a peak in the out-of phase susceptibility contain a significant fraction of SP grains. This behavior is observed for the re-melted samples, at temperatures around 100°K, suggesting the presence of an SP phase, in agreement with the analysis of hysteresis parameters.

Low-temperature remanence memory of TRM was measured through a complete cooling–heating cycle from 300°K to 10°K back to 300°K (Fig. 5a). All but two samples retain more than 99% of their TRM, whereas samples IS26E and IS26I lose 5% and 10% of TRM, respectively. This reversible behavior is attributed to elongated single-

Please cite this article as: Shaar, R., et al., Testing the accuracy of absolute intensity estimates of the ancient geomagnetic field using copper slag material, Earth Planet. Sci. Lett. (2010), doi:10.1016/j.epsl.2009.12.022

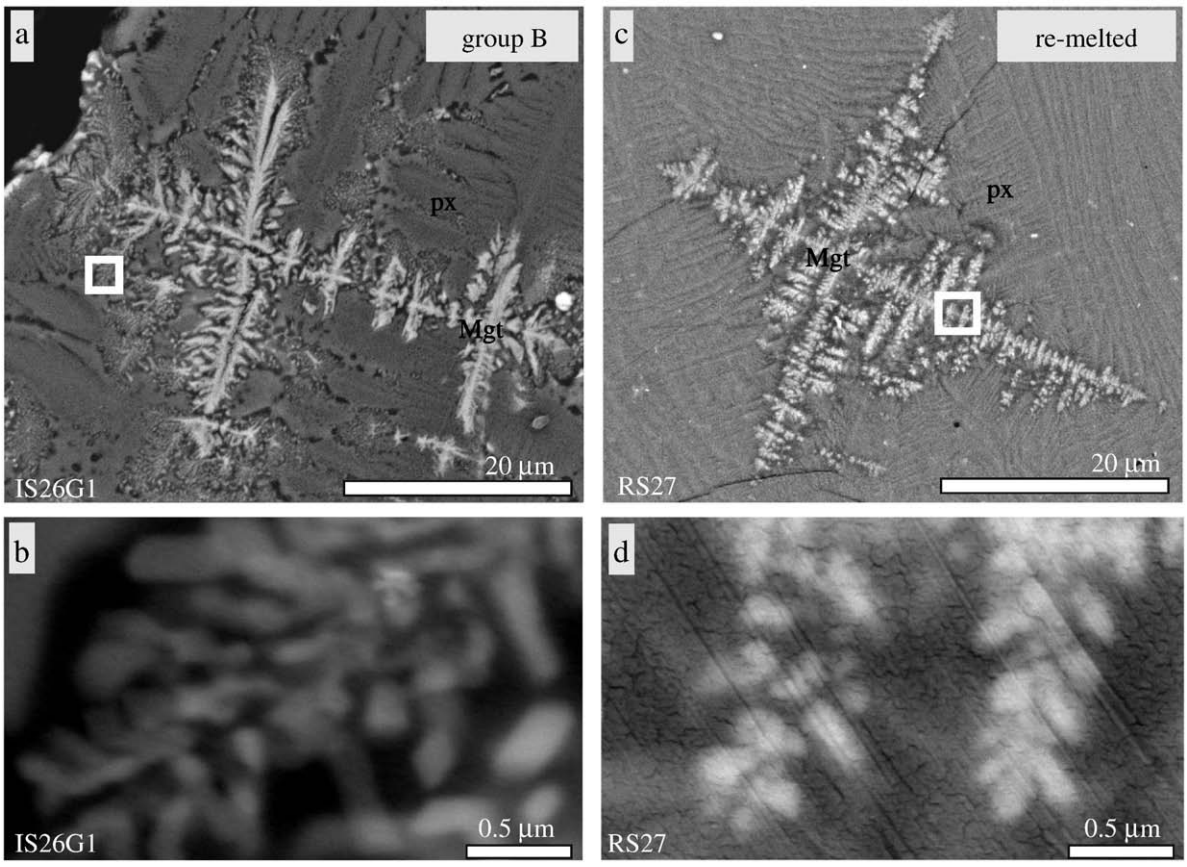

Fig. 3. Comparison between the dendritic texture of the group B slag (a,b) and that of laboratory-produced re-melted slag (c,d). 1:100,000 magnification (b,d) shows that a dendrite is composed of a large number of sub-micron elongated grains. The re-melted slag reproduces the distinctive texture found in the archaeological slag.

domain grains with dominant shape anisotropy (Dunlop and Özdemir, 1997). The less-single domain like behavior of samples IS26E and IS26I is in agreement with their relative position on a Day plot, again, supporting the analysis of the hysteresis data.

Results from magnetic and microscopic analyses argue that the samples are dominated by a shape-controlled, single-domain-like state. We interpret the domain states of the different sample groups as follows: 1) Group A is composed of SD or PSD grains, very close to pure SD range. 2) Group B is composed of SD or PSD grains, while samples IS26F and IS26G exhibit finer grains, closer to the SD range. 3) The re-melted slag is composed of two distinct populations: SD/PSD and SP, where the SP grains are not observed in the electron microscope images, because of the limited resolution of the SEM.

3.4. Behavior in Thellier experiments

Fig. 7a–e shows representative Arai plots (Nagata et al., 1963) from IZZI experiments on the slag samples. All plots show highly linear behavior, with reproducible pTRM checks. The unblocking temperature (T_{UB}) spectra of the samples are narrow, and show different ranges: 300–405 °C for Group A (Fig. 7a), 500–560 °C for Group B (Fig. 7b–e) and 485–534 °C for the re-melted slag (Fig. 7f). The T_{UB} spectra fall very close to the Curie temperatures estimated with the *K–T* curves (Table 1), supporting the interpretation of SD or fine PSD, given in Section 3.3. Orthogonal projections of the NRM, shown in the insets of Fig. 7, display a single-component of magnetization converging towards the origin.

Table 1
Summary of magnetic properties divided by groups and magnetic mineralogy.

Group	Sample	Magnetic mineralogy	T_c (*M–T*)[a]	T_c (*K–T*)[b]	T_{UB}[c]	MDF (mT)[d]	M_{rs}/M_s[e]	H_c (mT)[e]
A	IS26C	$Fe_{3-x}(Al,Mn,Mg)_xO_4$ $0.7<x<0.8$	332	376 (386)	300–405	25	0.45 ± 0.13	38 ± 7
B	IS26E	$Fe_{3-x}(Al,Mn,Mg)_xO_4$ $x\ll1$	534	552 (564)	500–560	40	0.19 ± 0.03	49 ± 3
	IS26F		550	551 (560)	500–560	$\gg90$	0.31 ± 0.01	81 ± 9
	IS26G		554	555 (563)	500–560	$\gg90$	0.32 ± 0.01	82 ± 5
	IS26I		533	552 (557)	500–550	50	0.22 ± 0.01	43 ± 1
Re-melted	RS25,RS26,RS27		521	515 (528)	485–535	45	0.01–0.15[f]	0.5–15[f]

[a] Curie temperature estimated from strong-field thermomagnetic curves.
[b] Curie temperature estimated from maximum in first (second) derivative of low-field susceptibility curves.
[c] Blocking temperature spectrum obtained from IZZI experiments.
[d] Median destructive field obtained from AF demagnetization of NRM.
[e] Averaged values calculated from room-temperature hysteresis parameters of four specimens that underwent Thellier experiments.
[f] Minimum and maximum values calculated from room-temperature hysteresis parameters.

Please cite this article as: Shaar, R., et al., Testing the accuracy of absolute intensity estimates of the ancient geomagnetic field using copper slag material, Earth Planet. Sci. Lett. (2010), doi:10.1016/j.epsl.2009.12.022

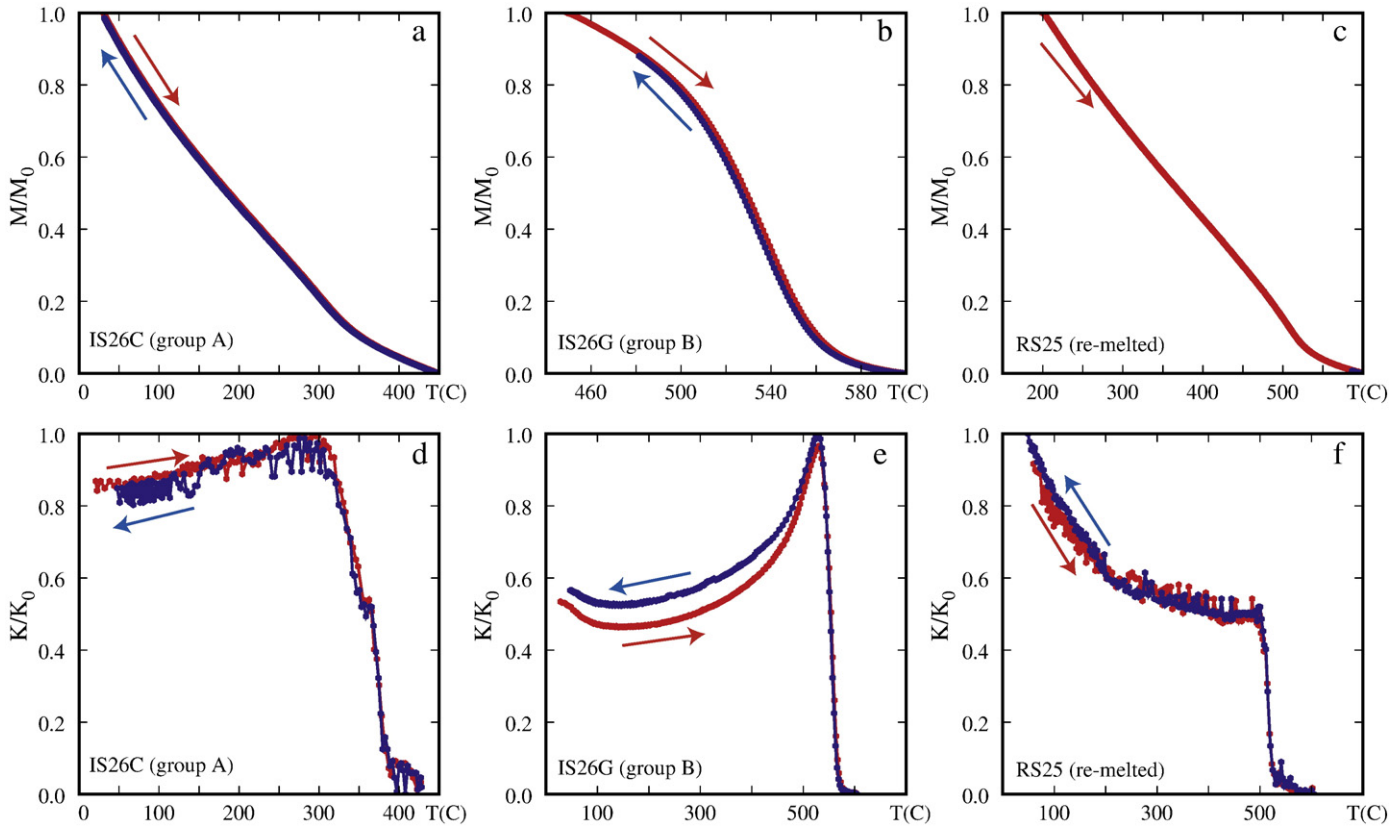

Fig. 4. Measurements of magnetization (M–T) and susceptibility (K–T) as a function of temperature for representative specimens from group A (a,d), group B (b,e) and the re-melted slag (c,f). Red (blue) lines denote heating (cooling). All curves are reversible, suggesting little alteration during heating. The M–T curves are dominated by the paramagnetic signal contributed by the silicate matrix, whereas the K–T curves show a sharp drop at T_c. (For interpretation of the references to colour in this figure legend, the reader is referred to the web version of this article.)

Table 2 lists the results of the IZZI experiments on the re-melted samples. Zigzagged behaviors of the Arai plots were observed for four specimens ($Z>0$ in Table 2). The zigzag is unique to the IZZI protocol and indicates a violation of an assumption important to the successful application of the Thellier method: that remanence is carried by ideal SD grains. As for specimens RS26c, RS27a and RS27f, the dominant zigzag is observed when the angle between the NRM and the oven's field (α in Table 2) is close to 180°, and the intensity of the expected field is higher than the oven field ($B_a/B_o>1$ in Table 2). The dependence of the degree of the zigzag on B_a/B_o and α is in agreement with the prediction of recent numerical models of the IZZI protocol (Yu et al., 2004; Yu and Tauxe, 2005; Biggin, 2006). The zigzag behavior of specimen RS27b is observed for $\alpha=5°$, implying higher degree of non-single-domain behavior. To test the effect of the zigzag on intensity determination, we calculated the slope of the Arai plot using three methods: 1) taking all points for least-square fit calculation, 2) taking only the ZI points, and 3) taking only the IZ points. The difference in slope calculation using the three methods was insignificant for specimens with $Z>1$ (less than 4%), implying that the quality of the Arai plots for intensity calculations was not affected by the zigzags.

3.5. Intensity determinations

Intensity determinations of the re-melted slag specimens followed the method of calculation described in Tauxe (2009) using both TRM anisotropy and non-linear-TRM (NLT) corrections. The temperature intervals used for intensity calculations were chosen such that the "NRM lost" of the first and the last points were less than 5% and more than 95% of the initial NRM, respectively. Two specimens (RS26e and RS27j) were rejected due to low fraction of NRM involved in the linear segment of the Arai plot and high degree of alteration in the ATRM procedure (Section 2.5).

Table 2 lists the calculated intensities of samples RS25, RS26 and RS27 produced under laboratory field intensities of 30, 60 and 90 μT, respectively, together with some of the commonly used quality statistics. Averaged field intensities after anisotropy and NLT corrections are 28.6 ± 1.8 μT and 58.7 ± 1.6 μT for samples RS25 and RS26, respectively. Averaged intensity for sample RS27 is 84.1 ± 2.1 μT, if taking specimens analyzed using oven field of 40 μT, and 84.9 ± 3.5 μT, if taking specimens analyzed using oven field of 90 μT. The results demonstrate an accuracy of within ~5% when the oven's field intensity is similar to the expected intensity, and slightly lower accuracy of within ~6% for sample RS27 when the oven's field is weaker than the expected intensity.

Intensity estimates of the archaeological samples are listed in Table S1 in the supplementary material. Since NLT correction for sample IS26C was relatively significant, we repeated the IZZI experiment for five more specimens in an oven field of 80 μT, which is the intensity of the expected field. For the final intensity calculation we applied a selecting methodology similar to the one described in Ben-Yosef et al. (2008a,b) and Ben-Yosef et al. (submitted for publication), using a set of cutoff values of quality parameters as a selecting criterion. For choosing the cutoff values, we first calculated these values for the re-melted slag (Table 2), and then applied the threshold values as selecting criteria for the archaeological dataset, allowing minimum values of 0.05 and 1.6 for β and Z parameters respectively (Table 3). Four specimens did not pass these selecting criteria. The results demonstrate very good agreement within specimens, showing standard deviations of 2%, 8%, 1%, 3%, and 7% for samples IS26C,E,F,G,I, respectively. The less SD behavior of samples

Please cite this article as: Shaar, R., et al., Testing the accuracy of absolute intensity estimates of the ancient geomagnetic field using copper slag material, Earth Planet. Sci. Lett. (2010), doi:10.1016/j.epsl.2009.12.022

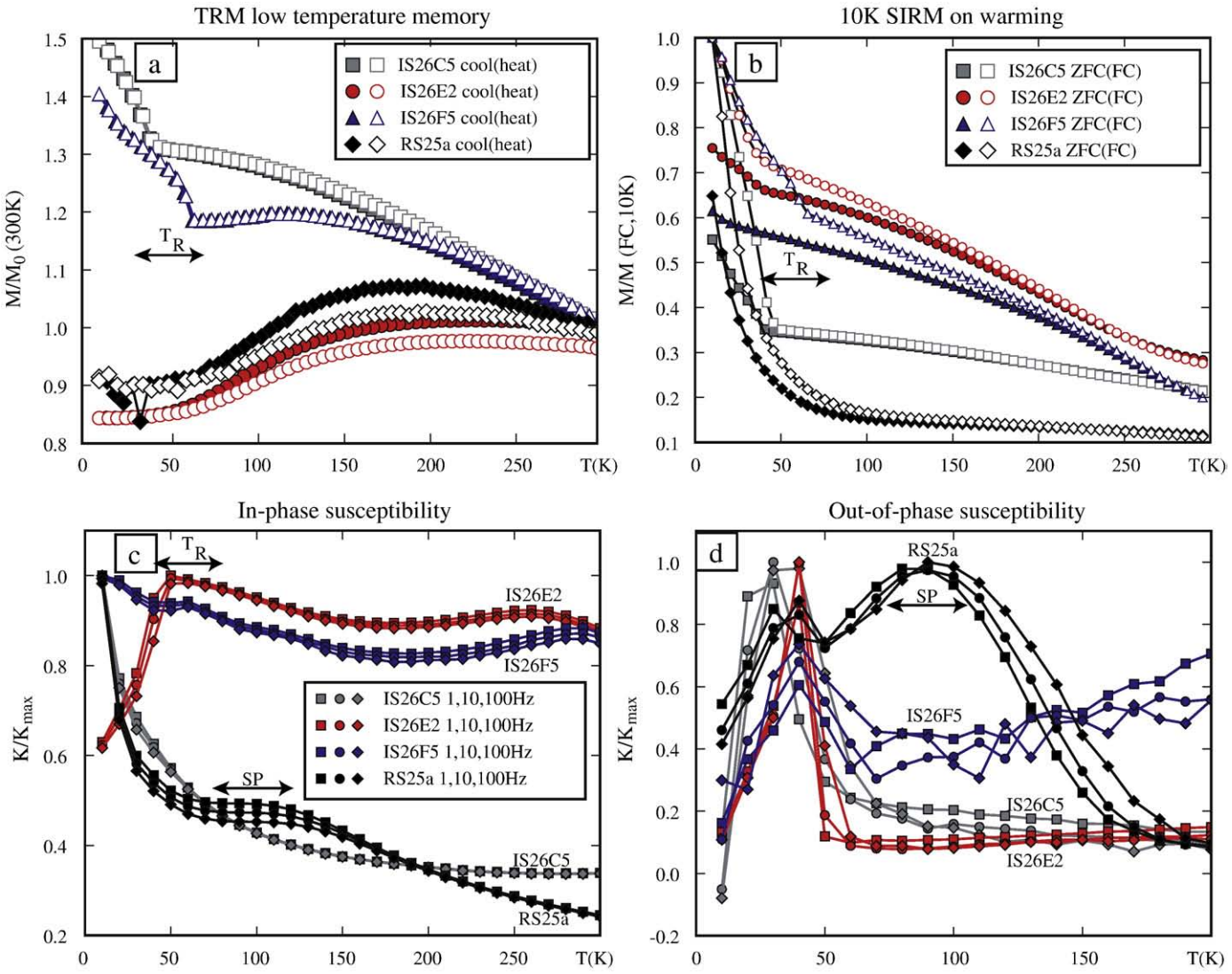

Fig. 5. Low-temperature measurements of representative specimens. (a) Low-temperature memory of TRM measured through a cooling–heating cycle from 300 K to 10 K and back to 300 K. (b) Warming curves of a 2T SIRM acquired at 10 K. ZFC: cooling from 300 K to 10 K in zero field. FC: cooling in 2T field. In-phase (c) and out-of-phase (d) susceptibility in various frequencies. T_R marks an abrupt change in remanence and susceptibility. SP indicates evidence of superparamagnetic behavior.

IS26E and IS26I, observed in the rock magnetic analysis (Section 3.3) is in agreement with the paleointensity statistics (Table S1), showing zigzag behaviors ($Z>0$), and a relatively higher value of standard deviations for samples IS26E and IS26I.

The entire dataset as well as our interpretations are available in the MagIC database (http://earthref.org).

4. Discussion

The objective of this paper is to rigorously investigate the precision and accuracy of archaeointensity estimates obtained from slag. The work aims at providing a firm basis for future archaeointensity studies of slag material, especially in southern Levant. The approach in this study was to divide the problem into two separate tests. In the first, we used electron microscopy and rock magnetic measurements to answer the question: "Does slag material display the magnetic properties required for valid Thellier experiments?" Our answer is discussed in Section 4.1. In the second test, we used laboratory-produced slag to answer the question: "What is the accuracy of the archaeointensity estimates derived from Thellier-style experiments on optimal samples?" Our answer is strikingly encouraging, and is discussed in Sections 4.2 and 4.3. The implications of this study extend beyond these two questions. While trying to answer the first question we improved our archaeological sampling technique, developed field and laboratory pre-selection tests, and deepened our understanding of the ancient technology of copper production. These advances are part of an ongoing research project and will be discussed in a separate paper together with a more complete archaeointensity study of Site Timna-30. While addressing the second question, we developed a unique experimental technique for testing the paleointensity method. We found that two important, albeit largely ignored, properties of remanence acquisition are critical for accurate intensity estimates: non-linear TRM acquisition at fields in the range of the Earth's, and TRM anisotropy in unexpected materials (e.g., those that did not flow or were not deformed). The effect of these properties on paleointensity estimates is discussed in Sections 4.4 and 4.5.

4.1. Can slag material be magnetically suitable for valid Thellier experiments?

The ferromagnetic phase in slag material occurs in a dendritic texture (Figs. 1–3). When viewed along two-dimensional polished surfaces, this dendritic assemblage appears to consist of a large number of individual sub-micrometers elongated particles arranged symmetrically in preferred orientations. However, EBSD measurements demonstrate that

Please cite this article as: Shaar, R., et al., Testing the accuracy of absolute intensity estimates of the ancient geomagnetic field using copper slag material, Earth Planet. Sci. Lett. (2010), doi:10.1016/j.epsl.2009.12.022

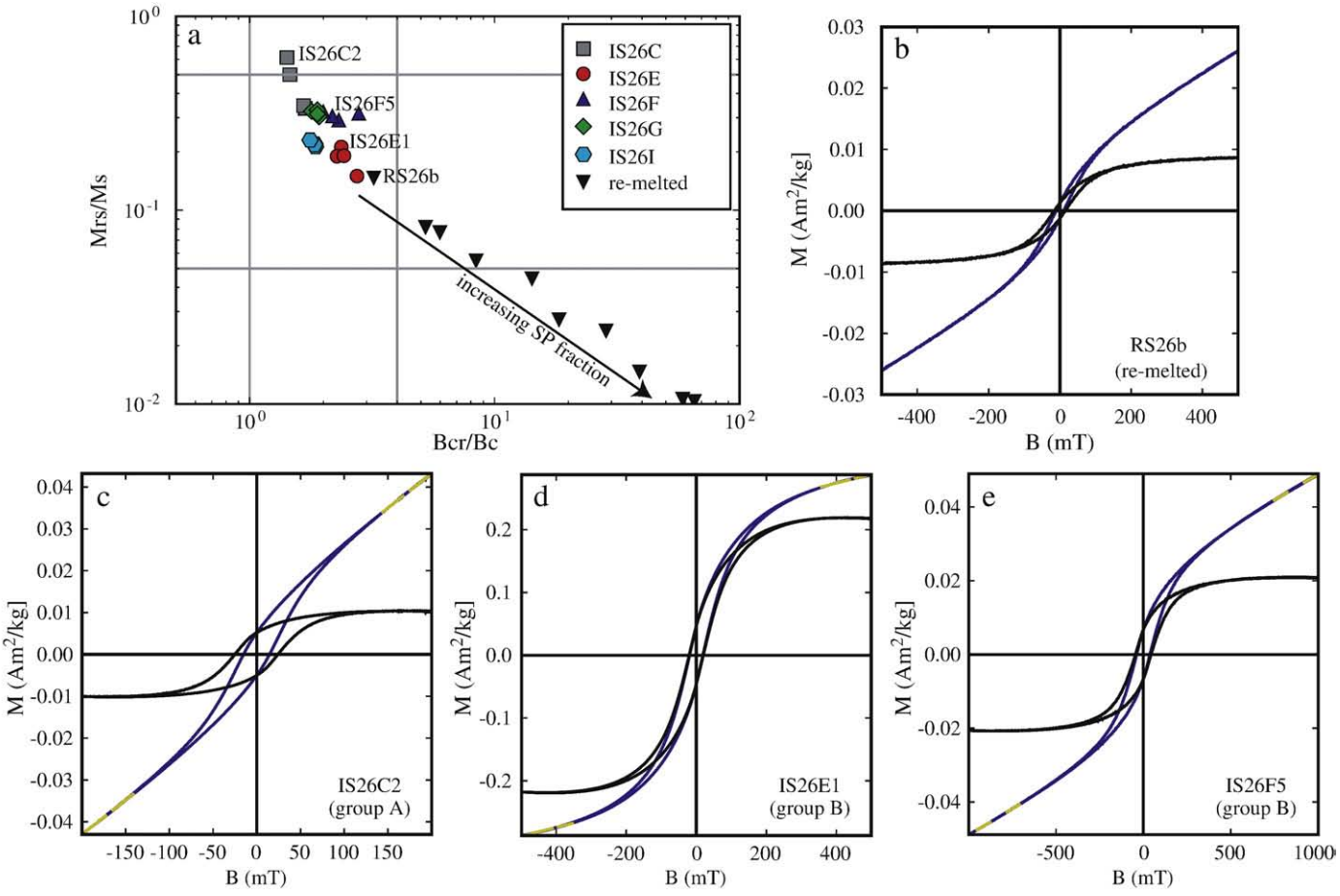

Fig. 6. Magnetic hysteresis results. (a) Hysteresis parameters displayed on a Day plot. "Re-melted" is assigned to samples RS25, RS26 and RS27 together (b)–(e) Representative major hysteresis loops for each group of samples. Blue loops indicate raw data, dashed yellow lines indicate the paramagnetic slope used to create the slope-adjusted major hysteresis loops shown in black. (For interpretation of the references to colour in this figure legend, the reader is referred to the web version of this article.)

all oxide particles within a dendritic assemblage have identical crystallographic orientations, indicating that these assemblages are actually joined, three-dimensional structures with a skeletal morphology common to rapidly quenched materials. The dimensions of each individual rod-shape branch suggest a shape-controlled single-domain-like state. The rock magnetic measurements support this interpretation, with two caveats: none of the samples fall within the SD field on a Day plot ($M_r/M_{rs}>0.5$), and the Arai plots of the re-melted slag are in cases slightly zigzagged. Taken together, rock magnetic analyses suggest a pseudo-single domain in a vortex or a flower state. Considering the behavior observed in the IZZI experiments and the rock magnetic analyses, we conclude that all the samples in this study are suitable for valid paleointensity experiments, i.e., they exhibit a pure thermoremanent magnetization carried by small PSD particles. Furthermore, because we performed the low-temperature analysis on replicate specimens, one that had undergone a full Thellier experiment and another that had never been heated (Section 2.4), and from the reversibility of the high-temperature curves (Fig. 4), we further conclude that slag is stable on heating, and does not tend to alter during Thellier experiments.

Groups A and B differ in the chemical composition of the remanence carriers. This difference is a result of the evolution of smelting technology throughout different archaeological periods. Slag samples from group A were produced from rocks poor in Fe and rich in Mn. The slag created from these rocks contains an uncommon magnetic mineralogy of Mn–Fe oxides. Mn–Fe oxides are rare, but not altogether unheard of in the rock magnetic literature, mainly because they are typically not the dominant magnetic phase. Here we offer a special case study of a strong TRM carried by a cubic ferromagnetic mineral with a chemical composition close to that of jacobsite, in a single-domain or pseudo-single domain state. This mineral is characterized by low blocking temperatures, low-coercivity, and a strong saturation remanence. Typically, magnetizations with low-coercivity spectra and low blocking temperatures are interpreted as a low-quality "soft" remanence, attributed to a MD state. However, we show here that the "low blocking temperature" remanence held by a population of SD Mn–Fe oxides is highly suitable for Thellier experiments.

4.2. What is the accuracy of archaeointensity calculations using suitable samples?

Estimation of the accuracy and precision of absolute intensity determinations is a fundamental problem discussed in many previous paleointensity studies (e.g. Coe et al., 1978; Aitken et al., 1988; Selkin and Tauxe, 2000; Valet, 2003; Donadini et al., 2007; Genevey et al., 2008). Theoretical or numerical treatments are not sufficient solely because the physical process of TRM acquisition is not completely understood (Fabian, 2001; Leonhardt et al., 2004; Xu and Dunlop, 2004; Yu et al., 2004; Biggin, 2006; Tauxe, 2009). Experimental approaches are often limited by the ability to reproduce exactly the conditions of material formation and TRM acquisition. These conditions were previously satisfied by applying a simulation of TRM on synthetic samples or on natural samples after they have undergone a pre-treatment procedure (Xu and Dunlop, 2004; Dunlop et al., 2005; Yu and Tauxe, 2005; Biggin and Poidras, 2006). An alternative

Please cite this article as: Shaar, R., et al., Testing the accuracy of absolute intensity estimates of the ancient geomagnetic field using copper slag material, Earth Planet. Sci. Lett. (2010), doi:10.1016/j.epsl.2009.12.022

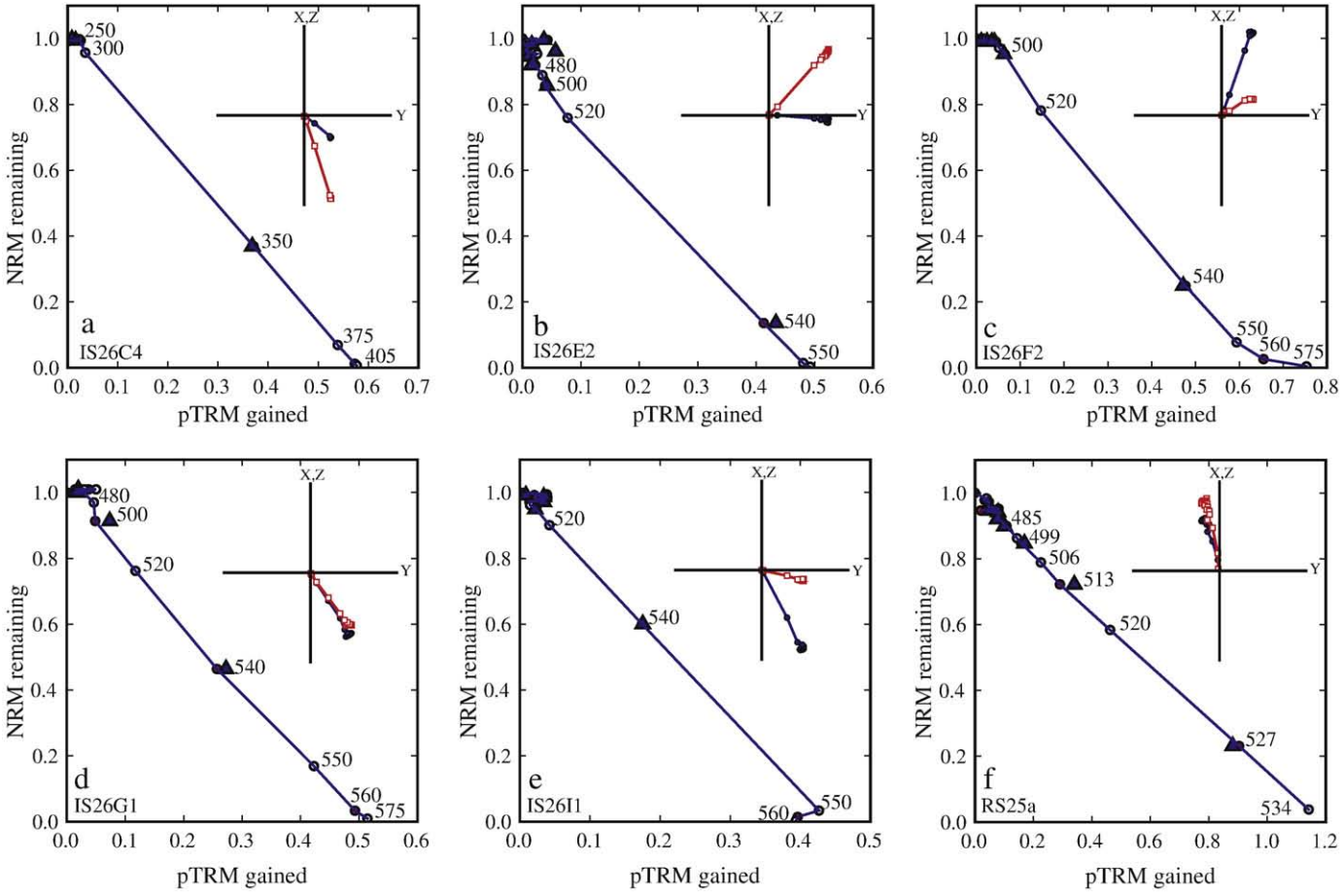

Fig. 7. Selected Arai plots of the archaeological slag (a–e) and the re-melted slag (f). Open (closed) circles are the Infield–Zerofield (Zerofield–Infield) steps of the IZZI experiments (Tauxe and Staudigel, 2004). pTRM check, performed every second temperature step are shown as triangles. All plots are highly linear. Orthogonal projections in the insets show convergence of NRM toward the origin. Red squares show projection on the *XZ* plane, blue circles show projection on the *YZ* plane in specimen coordinates. (For interpretation of the references to colour in this figure legend, the reader is referred to the web version of this article.)

approach uses "field tests" on historical lava flows or modern baked-clay artifacts formed under a known field (e.g., Calvo et al., 2002; Coe et al., 2004; Chauvin et al., 2005). In all these cases, tests have a limited control on the source material's magnetic properties and the field intensity in which the material was cooled. As a consequence, the fundamental issue of accuracy is still debated, especially when

Table 2
Results of IZZI experiments on the re-melted slag samples.

Specimen	B_a[a] (μT)	B_o (μT)	$T_{min}-T_{max}$ (°C)	α (°)	$f(f_{VDS})$	β	g	q	Z	DA	DR	B_{raw} (μT)[b]		B_{ani} (μT)		$B_{ani+NLT}$ (μT)	
RS25a	30	40	0–534	31	0.97(0.75)	0.01	0.79	63.7	0	0.9	2.4	34.3	29.1 ± 3.1	31.0	28.9 ± 1.5	30.8	28.6 ± 1.6
RS25b			0–534	178	1.00(0.94)	0.02	0.80	42.1	0	0.2	2.8	29.2		29.3		29.3	
RS25c			0–534	89	0.99(0.59)	0.02	0.78	33.8	0	1.8	2.9	27.5		28.4		28.2	
RS25d			0–534	45	0.99(0.71)	0.01	0.76	126.7	0	1.2	8.6	27.6		28.8		28.5	
RS25e			0–520	170	0.94(0.86)	0.02	0.78	49.0	0	0.8	7.2	27.0		26.8		26.4	
RS26a	60	40	0–527	114	1.00(0.64)	0.02	0.84	34.8	0	1.3	1.1	54.5	56.7 ± 2.0	54.8	57.7 ± 2.1	56.6	58.7 ± 1.6
RS26b			0–534	10	0.99(0.92)	0.01	0.79	131.4	0	0.3	11	57.7		57.8		58.5	
RS26c			0–534	173	1.02(0.92)	0.02	0.84	42.5	1.2	0.2	1.6	59.0		59.7		60.1	
RS26d			0–534	108	0.99(0.7)	0.03	0.78	28.7	0	1.6	2.8	55.5		58.5		59.7	
RS27a	90	40	0–520	175	1.01(0.98)	0.02	0.80	35.0	1.1	0.0	4.2	74.0	78.5 ± 3.9	74.3	78.3 ± 2.5	82.3	84.1 ± 2.1
RS27b			0–527	5	1.00(0.94)	0.01	0.86	71.5	1.2	0.3	7.6	79.8		79.3		83.9	
RS27c			325–527	25	0.97(0.85)	0.01	0.78	62.4	0	0.2	13.5	78.2		78.1		81.9	
RS27d			0–520	32	1.02(0.88)	0.01	0.84	61.1	0	0.7	5	84.2		78.9		86.6	
RS27e			325–527	50	0.94(0.71)	0.03	0.78	29.1	0	2.1	13	76.2		80.9		86.0	
RS27f	90	90	0–550	173	1.02(0.99)	0.04	0.81	18.9	1.2	0.7	0	84.2	83.2 ± 4.9	85.5	84.9 ± 3.5		
RS27g			300–520	89	0.98(0.95)	0.02	0.79	33.8	0	1.0	3	85.1		86.5			
RS27h			460–527	5	0.88(0.91)	0.02	0.75	43.7	0	1.1	3.9	87.5		87.7			
RS27i			0–527	50	0.98(0.95)	0.02	0.77	37.7	0	0.4	6.8	76.1		79.7			

[a] B_a—intensity of ambient field on production; B_o—intensity of the field used in the paleointensity oven; T_{min}–T_{max}—temperature interval for intensity calculation; α—angle between B_a and B_o; $f(f_{VDS})$—remanence fraction (Coe et al., 1978) (fraction of the total remanence (Tauxe and Staudigel, 2004)); β — scatter parameter (Coe et al., 1978); g—gap factor (Coe et al., 1978); q—quality factor (Coe et al., 1978); Z—the degree of zigzag of the Arai plot (Ben-Yosef et al., 2008a; Tauxe, 2009); DA—The Deviation of the ANGle (DANG; Tauxe and Staudigel, 2004); DR—The Difference RATio Sum (DRATS, Tauxe and Staudigel, 2004); B_{raw}—calculated intensity; B_{ani}—intensity corrected for anisotropy; $B_{ani+NLT}$,—intensity corrected for anisotropy and NLT.

[b] Confidence bounds on samples averages were determined by the standard deviation around the sample mean.

Please cite this article as: Shaar, R., et al., Testing the accuracy of absolute intensity estimates of the ancient geomagnetic field using copper slag material, Earth Planet. Sci. Lett. (2010), doi:10.1016/j.epsl.2009.12.022

Table 3
Cutoff values of quality criteria.

	f[a]	f_{VDS}	β	g	q	MAD	DA	DR	Z
This study: re-melted slag[b]	0.75	0.6	0.04	0.9	19	8	4	14	1.2
This study: archaeological slag[c]	0.83	0.6	0.05	0.8	12	5	4	13	1.6
Ben-Yosef et al. (2008a,b)	–	0.5	0.08	–	–	5	7	18	2.0
Ben-Yosef et al. (submitted for publication)	–	0.7	0.1	–	–	10	10	20	–

[a] Quality parameters f, f_{VDS}, β, g, q, DA, DR, Z as in Table 2; MAD—maximum angle of deviation (Kirschvink, 1980).
[b] Cutoff values were calculated after choosing temperature intervals as explained in section 3.2.
[c] Calculated cutoff values of the re-melted samples were applied as selecting criteria for the archaeological samples.

comparing estimates derived from different materials and methods (e.g., Donadini et al., 2007; Genevey et al., 2008).

In this study, we applied different approaches for estimating the validity of our archaeointensity data. We reproduced re-melted slag in the laboratory under controlled fields, and applied exactly the same paleointensity procedure on the archaeological and the re-melted material. The results reveal an accuracy of within ~5% when the field used in the paleointensity oven is close to the expected intensity (Table 2). The accuracy is slightly lower (~6%) when the field used in the paleointensity oven is lower than the expected intensity. The results support recommendations of recent models of the IZZI protocol (Yu et al., 2004; Biggin, 2006) to use an oven field close as possible to the expected field.

4.3. Paleointensity quality statistics

Reliability of paleointensity estimates can be judged by a set of quality statistics as described in detail by Tauxe (2009). We calculated some of the commonly used statistics for the re-melted specimens that passed the selecting conditions listed in Section 2.5 (Table 2). Cutoff values are summarized in Table 3 together with the values used as selecting criteria in three data-sets of archaeological slag: this study, Ben-Yosef et al. (2008a,b), and Ben-Yosef et al. (submitted for publication). The re-melted slag in this study demonstrates relatively high values supporting its suitability for high-quality paleointensity calculations. Table 3 shows that carefully selected archaeological slag samples, such as those from site Timna-30 in this study, can demonstrate similar quality statistics as the re-melted slag. However, since stringent quality control criteria cannot by themselves ensure accurate calculations, we use the laboratory test as an independent conclusive evidence for the validity and accuracy of archaeointensity data obtained from the archaeological slag. In this study, we use tighter values of cutoff selection criteria compared to previous studies (i.e. Ben-Yosef et al., 2008a,b and Ben-Yosef et al., submitted for publication) simply because we improved samples selection prior the experiments.

4.4. TRM anisotropy of un-deformed material

The effect of remanence anisotropy has long been recognized as a primary cause for erroneous paleointensities (Rogers et al., 1979; Aitken et al., 1981). TRM anisotropy in archaeological baked-clay artifacts, in particular pottery and bricks, has been generally interpreted to be the result of the manufacturing process (Odah et al., 2001; Genevey and Gallet, 2002). For rocks, TRM anisotropy has been generally interpreted as a result of flow (Leonhardt et al., 2006) or strain (Selkin et al., 2000). The petrographic expression of TRM anisotropy has been attributed to elongated or flat magnetic particles arranged in a preferred orientations (Selkin et al., 2000). An exceptional case of TRM anisotropy, which is not related to strain or flow, is the case of oriented exsolved inclusions in silicate hosts (Feinberg et al., 2006).

Surprisingly, the TRM acquisition for the re-melted slag samples is significantly anisotropic, with τ_{max}/τ_{min}, ranging from 1.04 to 1.57, where τ_{max} and τ_{min} are the maximum and minimum eigenvalues of the anisotropy tensor. These results were initially surprising because the re-melted samples were not subjected to any flow regime or strain. In addition, no flow textures are observed in the SEM images. Therefore, the existing mechanisms typically invoked for TRM anisotropy are not valid in this case, and an alternative mechanism is required. We recall that the magnetic carriers in the slag occur as finely grown, three-dimensional dendritic structures (Figs. 1–3). These dendrites consist of thin (<1 μm), multiply diverging branches, arranged in orientations that reflect the fastest directions of crystal growth. This dendritic structure is the root cause of TRM anisotropy in these samples. It is possible that the orientation of the dendrites is not random, and is influenced by the ambient conditions during cooling, perhaps even responding to internal stresses induced during cooling. Additional factors controlling the growth of the dendritic structures may be the propagation of a cooling front, or the orientation of the ambient magnetic field. This style of TRM anisotropy, which is reported here for the first time, requires further study.

4.5. Non-linear TRM acquisition at low fields

The most fundamental assumption of the Thellier method is that the magnetization acquired by a rock is linearly related to the applied field for weak fields such as the earth magnetic field. This linear relationship is usually taken a-priori as valid, and it is rarely tested. Selkin et al. (2007) recently showed that this relation does not hold for all rock types at all field intensities. In some cases, a hyperbolic tangent function provides a much more accurate description. Using numerical simulations of Néel theory Néel (1955), Selkin et al. (2007) predicted violation of the linearity assumption at low fields for a narrow size range of large acicular grains in a single-domain state. Our magnetic and petrographic analysis shows that this condition is satisfied in slag, appearing in shape-controlled dendritic structures (Figs. 1–3).

Fig. 8 shows a typical result of NLT experiment at fields weaker than 100 μT. The results are best fit by a hyperbolic tangent function, rather

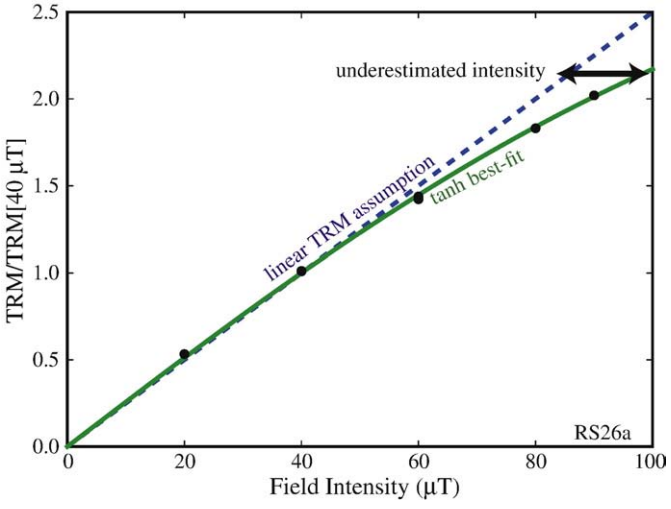

Fig. 8. Result of non-linear TRM experiment (NLT) displayed as TRM normalized by the TRM acquired at 40 μT versus field intensity. The blue dashed line represents the expected linear relationship assumed by the Thellier procedure. The green line shows best-fit hyperbolic tangent. The length of the arrow shows the extent of underestimated intensity due to the violation of the assumption of linear remanence acquisition. (For interpretation of the references to colour in this figure legend, the reader is referred to the web version of this article.)

Please cite this article as: Shaar, R., et al., Testing the accuracy of absolute intensity estimates of the ancient geomagnetic field using copper slag material, Earth Planet. Sci. Lett. (2010), doi:10.1016/j.epsl.2009.12.022

than a simple straight line. Therefore, we propose using the following procedure for paleointensity calculation, instead of a simple linear least-square fit of the Arai plot curve: Plot the NLT results as M/M (oven field) versus field intensity for several intensities, and fit data-points according to Eq. (1), as in Fig. 8.

$$M / M(\text{oven field}) = \alpha \cdot \tanh(\beta H) \quad (1)$$

Then, using Eq. (2), where b is the slope of the Arai plot,

$$b = M_{\text{anc}} / M_{\text{lab}} \quad (2)$$

calculate the result using Eq. (3), where H_{anc} is the ancient field intensity and F_a is the anisotropy correction factor.

$$H_{\text{anc}} = \tanh^{-1}[b \cdot F_a) / \alpha] / \beta \quad (3)$$

Table 2 shows that this calculation works very well for samples RS26 and RS27, which were originally produced using an ambient field intensities of 60 μT and 90 μT, respectively, and analyzed using an oven field of 40 μT.

NLT is significant for the re-melted slag and group A slag, but much less significant for group B slag. Fig. 3 shows that group B and re-melted slag share similar textures, but a still unresolved question is why the NLT effect is stronger for the re-melted slag? The answer could be related to the different chemical compositions of the two groups. The chemical compositions of group B are closer to stoichiometric magnetite, whereas the re-melted slag contains more impurities of Al, Mn, or Mg in the magnetite. Differences in the cooling geometry between the archaeological samples and the re-melted samples may offer another possible explanation for the variable extent of NLT.

5. Conclusions

(1) Slag material can be suitable for valid Thellier experiments in terms of magnetic mineralogy, type of magnetization and magnetic domain state. Slag can fulfill the assumptions underlying the Thellier method, i.e. it can carry a pure thermoremanence magnetization, which is carried exclusively by single-domain or fine pseudo-single-domain ferromagnetic particles.
(2) Laboratory tests of the Thellier method, using re-melted slag samples produced under controlled field intensities, demonstrate an accuracy of within ~5%, supporting the accuracy of the IZZI technique when using suitable samples.
(3) Non-linear TRM acquisition, and TRM anisotropy are important factors to monitor during paleointensity studies of slag material.
(4) Our experiments demonstrate that the theoretical hyperbolic–tangent relationship between TRM and applied field intensity can be important even at field strengths similar to Earth's and that the fundamental assumption of the Thellier method of a linear relationship between TRM and field intensity may be in error where certain types of material are concerned.
(5) The laboratory re-melted slag samples exhibit significant remanence anisotropy. According to our knowledge, it is the first reported geophysical evidence of magnetic anisotropy not caused by strain, flow, or subsolidus exsolution. We propose that the growth of the crystals as multiply diverging branches of dendrites arranged in preferred orientations is the root cause of the anisotropy.

Acknowledgements

We would like to thank Yosi Sherer and Andery Podlko from the Institute of Earth Sciences, the Hebrew University, for their technical support. We thank Vitaly Gutkin from the Unit for Nanoscopic Characterization of the Hebrew University for his assistance using SEM. We are grateful to Julie Bowles, Mike Jackson, and Peter Sølheid for their help during a Visiting Fellowship to the IRM, and to N. Seaton for help with the EBSD analysis. We thank the Israeli Antique Authority and Yuval Yekutiely for helping with the archaeological issues.

This study was supported by the US–Israel Binational Science Foundation Grant No. 2004/198, NSF grant EAR0636051, and Israel Science Foundation-FIRST program, grant no. 1334/05. The Institute for Rock Magnetism is supported by a grant from the Instrumentation and Facilities Program, Earth Science Division, the U.S. National Science Foundation (EAR-0732473).

Appendix A. Supplementary data

Supplementary data associated with this article can be found, in the online version, at doi:10.1016/j.epsl.2009.12.022.

References

Aitken, M.J., Alcock, P.A., Bussell, G.D., Shaw, C.J., 1981. Archaeomagnetic determination of the past geomagnetic intensity using ancient ceramics—allowance for anisotropy. Archaeometry 23, 53–64 (FEB).
Aitken, M.J., Allsop, A.L., Bussell, G.D., Winter, M.B., 1988. Determination of the intensity of the earth's magnetic-field during archaeological times—reliability of the Thellier technique. Rev. Geophys. 26 (1), 3–12.
Beard, J.S., Tracy, R.L., 2002. Spinels and other oxides in Mn-rich rocks from the Hutter Mine, Pitsylvania County, Virginia, U.S.A.: implications for miscibility and solvus relations among jacobsite, galaxite, and magnetite. Am. Mineral. 87, 690–698.
Ben-Yosef, E., Ron, H., Tauxe, L., Agnon, A., Genevey, A., Levy, T.E., Avner, U., Najjar, M., 2008b. Application of copper slag in geomagnetic archaeointensity research. J. Geophys. Res.-Solid Earth 113 (B8).
Ben-Yosef, E., Tauxe, L., Ron, H., Agnon, A., Avner, U., Najjar, M., Levy, T.E., 2008a. A new approach for geomagnetic archaeointensity research: insights on ancient metallurgy in the Southern Levant. J. Archaeol. Sci. 35 (11), 2863–2879.
Ben-Yosef, E., Tauxe, L., Levy, T.E., Shaar, R., Ron, H., Najjar, M., submitted for publication. Geomagnetic Intensity Spike Recorded in High Resolution Slag Deposit in Southern Jordan. Earth Planet. Sci. Lett. doi:10.1016/j.epsl.2009.09.001.
Biggin, A.J., 2006. First-order symmetry of weak-field partial thermoremanence in multi-domain (MD) ferromagnetic grains: 2. Implications for Thellier-type palaeointensity determination. Earth Planet. Sci. Lett. 245 (1-2), 454–470.
Biggin, A.J., Poidras, T., 2006. First-order symmetry of weak-field partial thermoremanence in multi-domain ferromagnetic grains. 1. Experimental evidence and physical implications. Earth Planet. Sci. Lett. 245 (1–2), 438–453.
Brachfeld, S.A., Hammer, J., 2006. Rock-magnetic and remanence properties of synthetic Fe-rich basalts: implications for Mars crustal anomalies. Earth Planet. Sci. Lett. 248 (3–4), 599–617.
Calvo, M., Prevot, M., Perrin, M., Riisager, J., 2002. Investigating the reasons for the failure of palaeointensity experiments: a study on historical lava flows from Mt. Etna (Italy). Geophys. J. Int. 149 (1), 44–63.
Carter-Stiglitz, B., Moskowitz, B., Solheid, P., Berquo, T.S., Jackson, M., Kosterov, A., 2006. Low-temperature magnetic behavior of multidomain titanomagnetites: TM0, TM16, and TM35. J. Geophys. Res.-Solid Earth 111 (B12).
Chauvin, A., Roperch, P., Levi, S., 2005. Reliability of geomagnetic paleointensity data: the effects of the NRM fraction and concave-up behavior on paleointensity determinations by the Thellier method. Phys. Earth Planet. Inter. 150 (4), 265–286.
Coe, R.S., Gromme, S., Mankinen, E.A., 1978. Geomagnetic paleointensities from radiocarbon-dated lava flows on Hawaii and question of Pacific nondipole low. J. Geophys. Res. 83 (NB4), 1740–1756.
Coe, R.S., Riisager, J., Plenier, G., Leonhardt, R., Krasa, D., 2004. Multidomain behavior during Thellier paleointensity experiments: results from the 1915 Mt. Lassen flow. Phys. Earth Planet. Inter. 147 (2–3), 141–153.
Day, R., Fuller, M., Schmidt, V.A., 1977. Hysteresis properties of titanomagnetites—grain-size and compositional dependence. Phys. Earth Planet. Inter. 13 (4), 260–267.
Donadini, F., Riisager, P., Korhonen, K., Kahma, K., Pesonen, L., Snowball, I., 2007. Holocene geomagnetic paleointensities: a blind test of absolute paleointensity techniques and materials. Phys. Earth Planet. Inter. 161 (1–2), 19–35.
Dunlop, D.J., Özdemir, O., 1997. Rock Magnetism: Fundamentals and Frontiers. Cambridge Univ. Press, New York. 573 pp.
Dunlop, D.J., 2002. Theory and application of the Day plot (M_{rs}/M_s versus H_{cr}/H_c) 1. Theoretical curves and tests using titanomagnetite data. J. Geophys. Res.-Solid Earth 107 (B3).
Dunlop, D.J., Zhang, B.X., Özdemir, O., 2005. Linear and nonlinear Thellier paleointensity behavior of natural minerals. J. Geophys. Res.-Solid Earth 110 (B1).
Dunlop, D.J., Carter-Stiglitz, B., 2006. Day plots of mixtures of superparamagnetic, single-domain, pseudosingle-domain, and multidomain magnetites. J. Geophys. Res.-Solid Earth 111 (B12).
Essene, E., Peacor, D.R., 1983. Crystal chemistry and petrology of coexisting galaxite and jacobsite and other spinel solvi. Am. Mineral. 68, 449–455.
Fabian, K., 2001. A theoretical treatment of paleointensity determination experiments on rocks containing pseudo-single or multi domain magnetic particles. Earth Planet. Sci. Lett. 188 (1–2), 45–58.

Feinberg, J.M., Harrison, R.J., Kasama, T., Dunin-Borkowski, R.E., Scott, G.R., Renne, P.R., 2006. Effects of internal mineral structures on the magnetic remanence of silicate-hosted titanomagnetite inclusions: an electron holography study. J. Geophys. Res.-Solid Earth 111 (B12).
Fox, J.M.W., Aitken, M.J., 1980. Cooling-rate dependence of thermoremanent magnetization. Nature 283 (5746), 462–463.
Gallet, Y., Genevey, A., Courtillot, V., 2003. On the possible occurrence of 'archaeomagnetic jerks' in the geomagnetic field over the past three millennia. Earth Planet. Sci. Lett. 214 (1–2), 237–242.
Genevey, A., Gallet, Y., 2002. Intensity of the geomagnetic field in Western Europe over the past 2000 years: new data from ancient French pottery. J. Geophys. Res.-Solid Earth 107 (B11).
Genevey, A., Gallet, Y., Constable, C.G., Korte, M., Hulot, G., 2008. Archeoint: an upgraded compilation of geomagnetic field intensity data for the past ten millennia and its application to the recovery of the past dipole moment. Geochem. Geophys, Geosyst. 9.
Genevey, A., Gallet, Y., Rosen, J., Le Goff, M., 2009. Evidence for rapid geomagnetic field intensity variations in Western Europe over the past 800 years from New French archeointensity data. Earth Planet. Sci. Lett. 284 (1–2), 132–143.
Glatzmaier, G.A., Coe, R.S., Hongre, L., Roberts, P.H., 1999. The role of the earth's mantle in controlling the frequency of geomagnetic reversals. Nature 401 (6756), 885–890.
Gubbins, D., Jones, A.L., Finlay, C.C., 2006. Fall in earth's magnetic field is erratic. Science 312 (5775), 900–902.
Halgedahl, S.L., Day, R., Fuller, M., 1980. The effect of cooling rate on the intensity of weak-field TRM in single-domain magnetite. J. Geophys. Res. 85 (NB7), 3690–3698.
Johnson, C.L., Constable, C.G., Tauxe, L., 2003. Mapping long-term changes in earth's magnetic field. Science 300 (5628), 2044–2045.
Kirschvink, J.L., 1980. The least-squares line and plane and the analysis of paleomagnetic data. Geophys. J. R. Astron. Soc. 62 (3), 699–718.
Leonhardt, R., Krasa, D., Coe, R.S., 2004. Multidomain behavior during thellier paleointensity experiments: a phenomenological model. Phys. Earth Planet. Inter. 147 (2–3), 127–140.
Leonhardt, R., Matzka, J., Nichols, A.R.L., Dingwell, D.B., 2006. Cooling rate correction of paleointensity determination for volcanic glasses by relaxation geospeedometry. Earth Planet. Sci. Lett. 243 (1–2), 282–292.
Levy, T.E., Higham, T., Ramsey, C.B., Smith, N.G., Ben-Yosef, E., Robinson, M., Munger, S., Knabb, K., Schulze, J.P., Najjar, M., Tauxe, L., 2008. High-precision radiocarbon dating and historical biblical archaeology in Southern Jordan. Proc. Natl. Acad. Sci. U.S.A. 105 (43), 16460–16465.
Min'ko, N.I., Nevedomskii, V.A., Vagin, V.V., 1988. Crystallization in silicomanganese slag castings. Glass Ceram. 45 (3), 114–116.
Moskowitz, B.M., Jackson, M., Kissel, C., 1998. Low-temperature magnetic behavior of titanomagnetites. Earth Planet. Sci. Lett. 157 (3–4), 141–149.
Nagata, T., Arai, Y., Momose, K., 1963. Secular variation of the geomagnetic total force during the last 5000 years. J. Geophys. Res. 68, 5277–5282.
Néel, L., 1955. Some theoretical aspects of rock magnetism. Adv. Phys. 4, 191–243.
Odah, H., Hussain, A.G., Hoffmann, V., Soffel, H.C., El-Gamili, M., Deebes, H., 2001. Effect of magnetic anisotropy on the experimentally determined palaeointensity of the geomagnetic field. Earth Planets Space 53 (5), 363–371.
Ohashi, Y., 1984. Polysynthetically-twinned structures of enstatite and wollastonite. Phys. Chem. Miner. 10, 217–229.
Özdemir, O., Dunlop, D.J., Moskowitz, B.M., 1993. The effect of oxidation on the Verwey transition in magnetite. Geophys. Res. Lett. 20 (16), 1671–1674.
Rogers, J., Fox, J.M.W., Aitken, M.J., 1979. Magnetic-anisotropy in ancient-pottery. Nature 277 (5698), 644–646.
Rothenberg, B., 1980. Die Archaeologie Des Verhüttungslagers Site 30. In: Conrad, H.G., Rothenberg, B. (Eds.), Antikes Kupfer Im Timna-Tal, pp. 187–214.
Selkin, P.A., Tauxe, L., 2000. Long-term variations in palaeointensity. Philos. Trans. R. Soc. Lond. Ser. A-Math. Phys. Eng. Sci. 358 (1768), 1065–1088.
Selkin, P.A., Gee, J.S., Tauxe, L., Meurer, W.P., Newell, A.J., 2000. The effect of remanence anisotropy on paleointensity estimates: a case study from the Archean stillwater complex. Earth Planet. Sci. Lett. 183 (3–4), 403–416.
Selkin, P.A., Gee, J.S., Tauxe, L., 2007. Nonlinear thermoremanence acquisition and implications for paleointensity data. Earth Planet. Sci. Lett. 256 (1–2), 81–89.
Tarduno, J.A., Cottrell, R.D., Smirnov, A.V., 2006. The paleomagnetism of single silicate crystals: recording geomagnetic field strength during mixed polarity intervals, superchrons, and inner core growth. Rev. Geophys. 44 (1).
Tauxe, L., 1998. Paleomagnetic Principles and Practice. Kluwer Academic Publishers. 299 pp.
Tauxe, L., Staudigel, H., 2004. Strength of the geomagnetic field in the cretaceous normal superchron: new data from submarine basaltic glass of the troodos ophiolite. Geochem. Geophys. Geosyst. 5.
Tauxe, L., 2006. Long-term trends in paleointensity: the contribution of DSDP/ODP submarine basaltic glass collections. Phys. Earth Planet. Inter. 156 (3–4), 223–241.
Tauxe, L., Yamazaki, T., 2007. Paleointensities. In: Schubert, G. (Ed.), Treatise on Geophysics, vol. 5. Elsevier, pp. 509–564.
Tauxe, L., 2009. Essentials of Paleomagnetism, University of California Press, in press, Web Edition: http://magician.ucsd.edu/Essentials/.
Thellier, E., Thellier, O., 1959. Thellier, Sur L'intensité Du Champ Magnétique Terrestre Dans Le Passé Historique Et Géologique. Ann. Geophys. 15, 285–378.
Valet, J.P., 2003. Time variations in geomagnetic intensity. Rev. Geophys. 41 (1).
Vautier, R., Paulus, M., 1970. Magnetic and other properties of oxides and related compounds. In: Part, B, Hellwege, K.H., Hellwege, A.M. (Eds.), Landolt-Börnstein—Group III Condensed Matter 4b. Springer-Verlag, Berlin, pp. 158–160.
Worm, H.U., Jackson, M., 1999. The superparamagnetism of Yucca Mountain Tuff. J. Geophys. Res.-Solid Earth 104 (B11), 25415–25425.
Xu, S., Dunlop, D.J., 2004. Thellier paleointensity theory and experiments for multidomain grains. J. Geophys. Res.-Solid Earth 109 (B7).
Yu, Y.J., Tauxe, L., Genevey, A., 2004. Toward an optimal geomagnetic field intensity determination technique. Geochem. Geophys. Geosyst. 5.
Yu, Y.J., Tauxe, L., 2005. Testing the IZZI protocol of geomagnetic field intensity determination. Geochem. Geophys. Geosyst. 6.

Please cite this article as: Shaar, R., et al., Testing the accuracy of absolute intensity estimates of the ancient geomagnetic field using copper slag material, Earth Planet. Sci. Lett. (2010), doi:10.1016/j.epsl.2009.12.022